PNAS RESEARCH ARTICLE | EARTH, ATMOSPHERIC, AND PLANETARY SCIENCES OPEN ACCESS

Unexpected increase of the deuterium to hydrogen ratio in the Venus mesosphere

Arnaud Mahieux[a,b,1], Sébastien Viscardy[a], Roger Vincent Yelle[c], Hiroki Karyu[d], Sarah Chamberlain[a], Séverine Robert[a], Arianna Piccialli[a], Loïc Trompet[a], Justin Tyler Erwin[a], Soma Ubukata[d], Hiromu Nakagawa[d], Shungo Koyama[d], Romain Maggiolo[a], Nuno Pereira[a], Gaël Cessateur[a], Yannick Willame[a], and Ann Carine Vandaele[a]

Affiliations are included on p. 8.

Edited by Jonathan Lunine, Cornell University, Ithaca, NY; received January 24, 2024; accepted July 3, 2024

This study analyzes H_2O and HDO vertical profiles in the Venus mesosphere using Venus Express/Solar Occultation in the InfraRed data. The findings show increasing H_2O and HDO volume mixing ratios with altitude, with the D/H ratio rising significantly from 0.025 at ~70 km to 0.24 at ~108 km. This indicates an increase from 162 to 1,519 times the Earth's ratio within 40 km. The study explores two hypotheses for these results: isotopic fractionation from photolysis of H_2O over HDO or from phase change processes. The latter, involving condensation and evaporation of sulfuric acid aerosols, as suggested by previous authors [X. Zhang *et al.*, *Nat. Geosci.* 3, 834–837 (2010)], aligns more closely with the rapid changes observed. Vertical transport computations for H_2O, HDO, and aerosols show water vapor downwelling and aerosols upwelling. We propose a mechanism where aerosols form in the lower mesosphere due to temperatures below the water condensation threshold, leading to deuterium-enriched aerosols. These aerosols ascend, evaporate at higher temperatures, and release more HDO than H_2O, which are then transported downward. Moreover, this cycle may explain the SO_2 increase in the upper mesosphere observed above 80 km. The study highlights two crucial implications. First, altitude variation is critical to determining the Venus deuterium and hydrogen reservoirs. Second, the altitude-dependent increase of the D/H ratio affects H and D escape rates. The photolysis of H_2O and HDO at higher altitudes releases more D, influencing long-term D/H evolution. These findings suggest that evolutionary models should incorporate altitude-dependent processes for accurate D/H fractionation predictions.

Venus | mesosphere | HDO/H_2O ratio | water cycle | remote sensing observations

Significance

Studying Venus's HDO and H_2O sheds light on its water history. The HDO/H_2O ratio in its bulk atmosphere, 120 times Earth's, suggests a significantly wetter past for Venus. Our study analyzes mesospheric (70 to 110 km) temperature, H_2O, and HDO profiles taken in solar occultation by SOIR/Venus Express. We observe increasing relative abundances of both isotopologues and a significant D/H ratio rise with altitude. This finding challenges previous assumptions about upper-mesosphere H and D abundances available for escape, impacting atmospheric evolution models. We propose a cycle mechanism involving water fractionation during condensation into the sulfur-based aerosols, evaporation, and transport in the mesosphere between warm and cold regions to explain our finding, which is consistent with the observed SO_2 inversion layer.

Although Venus is sometimes referred to as Earth's twin, its current surface conditions are drastically different, making it inhospitable to life. Not only is liquid water unable to exist due to the extreme temperatures and pressures beneath the thick cloud layer (~45 to ~65 km), but more importantly, it is nearly absent from the Venusian atmosphere, which contains only 30 ± 10 parts per million by volume (ppmv) of water vapor below 15 km (1). To put this into perspective, these altitudes have 150,000 times less water than comparable altitudes on Earth (2). Above the cloud layer, the water content is much lower, with measurements indicating a few ppmv (3–7). The pronounced decrease in the H_2O volume mixing ratio (VMR) within the cloud layer can be attributed to the hydration of sulfuric acid aerosols in the clouds, which effectively trap most of the water (8). Moreover, this water scarcity is accompanied by a significant enrichment in deuterium; the D/H ratio in water within the ~30 to 70 km altitude range is around 120 times higher than that observed in Earth's oceans (Vienna Standard Mean Ocean Water, VSMOW = 1.5567×10^{-4}) (3, 4, 9–12).

The inner planets, including Venus and Earth, formed in a region of the protoplanetary disk where temperatures were too high for volatiles like water to condense. Water in the disk was rich in deuterium, with the deuterium to hydrogen (D/H) ratios ranging from 10^{-3} to 10^{-2} (see, e.g., ref. 13 and references therein). When H_2O is transported to the hot inner region surrounding the Sun, isotopic exchange reactions with molecular hydrogen (H_2) drastically reduced its D/H ratio to $\sim 2 \times 10^{-5}$, or ~0.06 VSMOW (14). Moreover, the isotopic exchange reactions become less efficient at the lower temperatures found beyond the snow line (15). It is thus believed that water-rich carbonaceous chondrites from the outer asteroid belt, which have a mean D/H ratio similar to Earth's, likely served as the primary sources of water for the inner planets during the solar system formation (see ref. 13, and references therein). It follows that, like Earth, Venus probably experienced impacts from such planetesimals, which would result in an initial D/H ratio similar to

Author contributions: A.M. designed research; A.M., S.V., R.V.Y., H.K., and J.T.E. performed research; A.M. and S.V. contributed new reagents/analytic tools; A.M., S.C., S.R., A.P., L.T., S.U., H.N., S.K., R.M., N.P., G.C., Y.W., and A.C.V. analyzed data; A.C.V. is the PI of the SOIR instrument; and A.M., S.V., R.V.Y., S.R., A.P., L.T., R.M., and A.C.V. wrote the paper.

The authors declare no competing interest.

This article is a PNAS Direct Submission.

[1]To whom correspondence may be addressed. Email: arnaud.mahieux@aeronomie.be.

This article contains supporting information online at https://www.pnas.org/lookup/suppl/doi:10.1073/pnas.2401638121/-/DCSupplemental.

Published August 12, 2024.

that found in Earth's oceans. This hypothesis is further supported by the fact that other volatiles, such as carbon and nitrogen inventories, are comparable between Venus and Earth (2).

For these reasons, some studies show that Venus initially held substantially more water than it does today and that the planet would have undergone an extraordinary runaway greenhouse sometime in its history. In this scenario, water would have been a key greenhouse gas (e.g., ref. 2, and references therein). On early Venus, liquid water would have gradually evaporated, resulting in high vapor abundances in the atmosphere up to altitudes where efficient photodissociation occurs. This process would have been followed by the preferential escape of hydrogen atoms over deuterium, its heavier isotope, leading to an increase in the D/H ratio of water in Venus' atmosphere (2, 16). Conversely, other studies suggest that the current deuterium levels could be achieved without requiring a wetter Venus in the past (17).

The mesosphere of Venus appears to be a critical region where complex, interconnected processes regulate the amounts of water isotopologues (H_2O and HDO) that can reach altitudes where hydrogen and deuterium atoms are released by photolysis. In this regard, it is important to note that the mesospheric water is closely linked to the sulfur cycle (see, e.g., ref. 18, and references therein). Carbonyl sulfide, OCS, chemically produced in the lower troposphere, is transported above the clouds by the Hadley cell circulation, along with sulfur dioxide (SO_2), though to a lesser extent. Upon reaching these altitudes, OCS gets oxidized and eventually produces sulfuric acid (H_2SO_4) in the presence of water vapor. This acid subsequently condenses with water to form hydrated aerosol particles, which contain over 75% of H_2SO_4 by mass (18). Additionally, allotropes, such as S_x, have also been explored as potential components of the aerosol particles as an explanation for the "unknown UV absorber" (19).

Observations (20) and models (21) show that the aerosols in the upper haze layer exhibit a bimodal distribution. These tiny droplets are transported upward either by diffusion or through hypothetical wind gusts (21), reaching altitudes above 90 km, where rising temperatures cause them to evaporate. At these altitudes, sulfuric acid, potentially present under supersaturated conditions (18), undergoes photochemical destruction, reverting to SO_2. This mechanism supports the increase of the SO_2 abundance observed above 80 km (22, 23).

Previous investigations have focused on the interaction between aerosols and related atmospheric processes, such as radiative-dynamical feedback and the effect of eddy diffusion on the structure of main cloud layers (24), although these works did not cover the altitude range of the upper haze layer. However, the water vapor profile is kept fixed over time in the models of refs. 18, 19, 21, and 25, ignoring the effect of evaporation and condensation on the background H_2O vapor profile. Recent microphysics simulations (26) included the upper haze layer up to 100 km and showed that H_2SO_4 vapor and H_2O vapor profiles are strongly influenced by the evaporation of the upper haze particles. We refer the reader to the extensive reviews available in these papers.

To understand the evolution of water in the Venusian atmosphere and its eventual loss to space, it is crucial to characterize the abundances of H_2O and HDO in the mesosphere. The Solar Occultation in the InfraRed (SOIR) instrument onboard the European Space Agency (ESA) Venus Express (VEx) spacecraft, operational from 2006 to 2014, provided valuable information for this purpose. Utilizing solar occultation, SOIR simultaneously recorded the vertical profiles of various species, including both water isotopologues (27). While these two isotopologues have been measured by ground-based telescopes at the cloud top or higher in the mesosphere, but not simultaneously (3, 4, 11, 12), previous studies reported the D/H ratio in mesospheric water only from the very first solar occultations performed early during the VEx mission (5, 28). Our study, analyzing the complete dataset of SOIR observations over the 8 y of operation, reveals a striking increase in the HDO/H_2O ratio in the ~65 to ~110 km altitude range—from 200 to 1,500 times that in Earth's oceans. These findings contribute to a better understanding of the processes driving hydrogen loss on Venus and provide valuable insights into the evolution of its atmosphere.

The SOIR Instrument and the Inversion Code

The Solar Occultation in the InfraRed (SOIR) instrument, an infrared spectrometer on board the ESA VEx spacecraft, was dedicated to studying the composition of Venus' atmosphere in solar occultation. It recorded radiance spectra in four different tunable spectral regions at a 1 Hz rate as the Sun was setting or rising, as seen from VEx. Due to this observation geometry, all observations occurred at the Venus terminator near 6 AM or 6 PM local solar time (LST). SOIR was sensitive in the 2.2 to 4.4 μm spectral range (2,200 to 4,400 cm^{-1}), where many key species present absorption spectral features used to determine their abundances. The complete database on temperature, CO_2, CO, H_2O, HDO, HCl, HF, SO_2, SO_3, OCS, CS, and CS_2 number densities is described in refs. 27 and 29. *SI Appendix*, section A provides more details about the SOIR instrument.

The spectral inversion code, ASIMAT, is fully described in ref. 30. A concise summary is provided here. A two-step iterative procedure was implemented to derive the species number density and temperature vertical profiles. In the first step, the Bayesian Rodgers algorithm was used to calculate vertical number density profiles for each species absorbing in a set of spectra, i.e., for one order and one bin. They considered the Venus International Reference Atmosphere [VIRA (31)] as the a priori for the first step. The Voigt approximation for the absorption lines was considered with the spectroscopic parameters from HITRAN 2012, accounting for the spectral line atmospheric saturation to consider only the altitude regions where the instrument was sensitive to line intensities. At those altitudes, the pressure is sufficiently low, that there is no need to consider asymmetric line shapes such as sub-Lorentzian line profile (32). In the second step, the profiles of each species were combined using a weighted moving average from the four different orders and two bins. If CO_2 was among the measured species, which was nearly always the case, hydrostatic equilibrium was assumed to compute the temperature profile, considering VIRA's CO_2 VMR vertical profile. In the next iteration, the mean species vertical profiles were considered a priori together with the new temperature profile because of the large temperature dependence of the spectral lines in the infrared. Iterations were performed until the vertical profiles of all species were within the uncertainties of the previous step. Convergence was usually achieved within three to four iterations. A summary of the spectroscopy and a typical retrieval example can be found in *SI Appendix*, sections B and C, respectively.

Results

For this work, we consider occultations during which H_2O, HDO, and CO_2 (and thus temperature) were simultaneously retrieved: 344 individual observations meet this criterion, covering all latitudes and spanning the whole VEx mission from June 2006 until December 2014.

In Fig. 1 *A*–*C* and *E*, we present the CO_2, temperature, H_2O, and HDO number densities of all the considered orbits; the corresponding H_2O and HDO VMRs are given in Fig. 1 *D* and *F*. The individual profiles are provided as the gray profiles. The

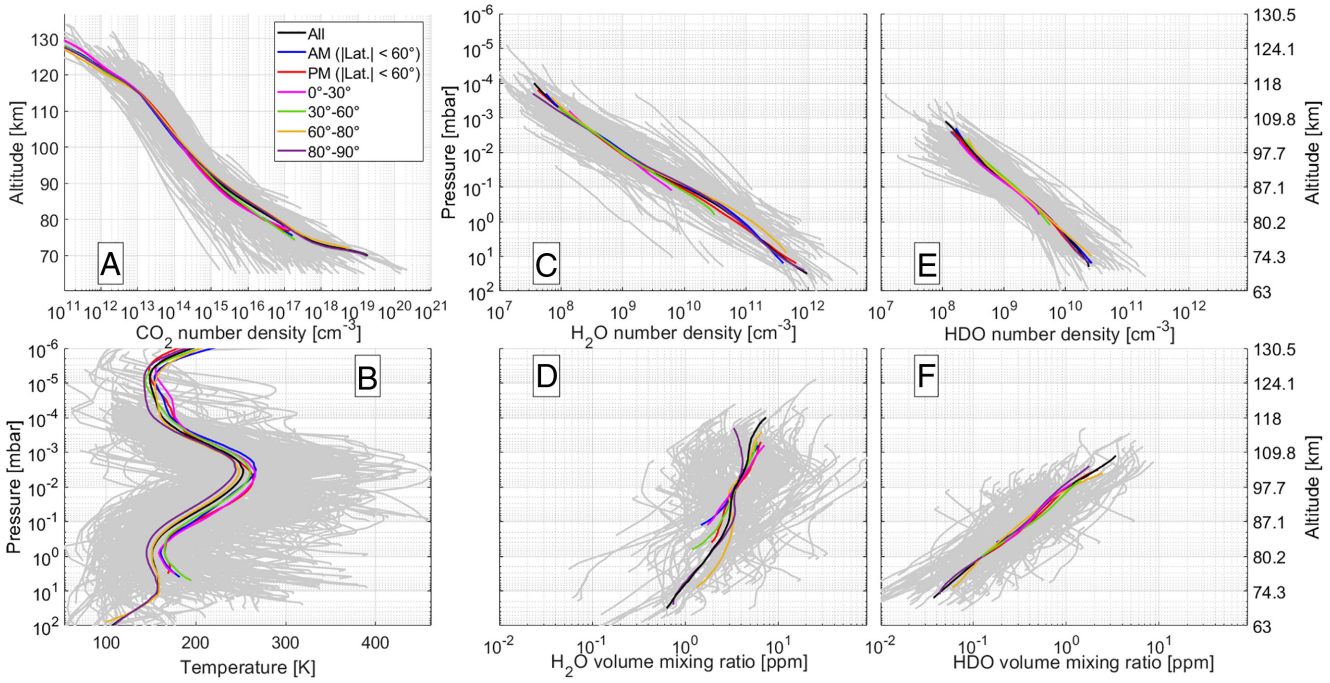

Fig. 1. CO_2 number density (Panel *A*), temperature (Panel *B*), H_2O number density (Panel *C*), H_2O VMR (Panel *D*), HDO number density (Panel *E*), and HDO VMR (Panel *F*) vertical profiles. The gray profiles are the individual profiles, while the colored profiles are averages for the whole database (black) as a function of the side of the terminator (blue for AM, red for PM, for absolute latitudes <60°), and by latitude bins (0 to 30° in pink, 30 to 60° in green, 60 to 80° in orange, and 80 to 90° in purple), while assuming equatorial symmetry. The uncertainties are not displayed for clarity of the figures; they range from 40% at 120 km to 14% at 100 km and increase to 50% below 80 km for H_2O, from 50% at 110 km and 15% between 90 and 70 km for HDO, and from 15 to 40% between 130 and 80 km and 40 to 60% between 80 and 65 km for CO_2.

averaged profiles for the morning and evening sides of the terminator (for absolute latitudes lower than 60°) and for absolute latitude bins (0° to 30°, 30° to 60°, 60° to 80°, and 80° to 90°), thus assuming North–South hemispheric symmetry, are the colored profiles. The uncertainties on the individual profiles are not displayed for clarity. They are of the same order of magnitude as those reported in the figures of *SI Appendix*, section C. The mean profiles are the same as those of ref. 27 and are discussed in that work.

To ease the comparison between the different observations perturbed by the bulk atmosphere variations induced by the atmospheric waves, we present the temperature and the H_2O and HDO densities and VMRs on a pressure scale. Hence, if we assume the CO_2 VMR from VIRA, we can compute the pressure vertical profile for each observation. The approximate altitudes for the different pressure levels are given on the right-hand side of Fig. 1 *E* and *F*. Considering the HDO and H_2O number density vertical profiles on a pressure scale instead of an altitude scale reduces the variability at any level by a factor of ~2. Still, large variations are observed for all three species, up to two orders of magnitude at any altitude level. This variability is observed for most species and has previously been noted in research papers by several instruments on board VEx: SPICAV/UV, SOIR, VIRTIS, and VeRa (ref. 33, and references therein).

In this work, we focus on the mean profiles. Fig. 2 presents the individual HDO/H_2O ratio profiles and the mean profiles for the same LST and latitude regions as in Fig. 1. The weighted variability for the mean profile of the whole database is also provided as the horizontal black lines. The equivalent D/H ratio is provided in the upper-axis using the relation

$$\frac{D}{H} = \frac{HDO}{HDO + 2H_2O}, \qquad [1]$$

as well as the factor to VSMOW. We note that a few percent bias in the D/H profile could be introduced because not all H_2O and HDO profiles reach the 10^{-3} mbar level; only those reaching larger densities at the top of the profiles do. However, this possible bias remains well within the weighted variability. For this reason, the mean D/H profiles above the 10^{-2} mbar level are set as dashed lines in Fig. 2.

Derived mole fractions are in agreement with previous results (5, 9, 10, 12, 28); however, a surprising result, first reported here, is the increase in the HDO/H_2O ratio by a factor larger than 10 from 70 to 108 km altitude.

The mean profiles are calculated on a pressure scale, considering the uncertainties on the mean profiles as weighting factors. The AM and PM profiles are similar, which indicates no terminator side dependence of the HDO/H_2O ratio. The mean value of the HDO/H_2O ratio varies between 0.052 ± 0.038 at ~70 km (20 mbar) and 0.62 ± 0.45 at ~108 km (1.2 μbar). This corresponds to a D/H ratio of 0.025 ± 0.019 at ~70 km and 0.24 ± 0.17 at ~108 km or 162 and 1519 times the VSMOW.

Similar to the LST dependence study, we do not see any significant variation in the HDO/H_2O ratio as a function of the absolute latitude since all profiles lie within the observed variability. We note that the 0° to 30° profile shape below the 2×10^{-2} mbar level is probably due to too little data available at these pressure levels.

The HDO/H_2O profiles from ref. 5 are reported in Fig. 2 and lie within the profiles presented in this work. We also note that the H_2O VMR profiles do not decrease with altitude, as observed in refs. 5 and 28. The likely explanation is twofold. First, they considered the total density and temperature from VIRA, while in this work, they are computed from the simultaneously measured CO_2 profiles. Second, these profiles were retrieved based on the same (much smaller) dataset discussed in this work. Moreover, many substantial differences have been implemented in the SOIR calibration pipeline and retrieval algorithm since 2008. This impacted the results as the calibration was not set, and the transmittance spectra were not correctly computed. This explains the

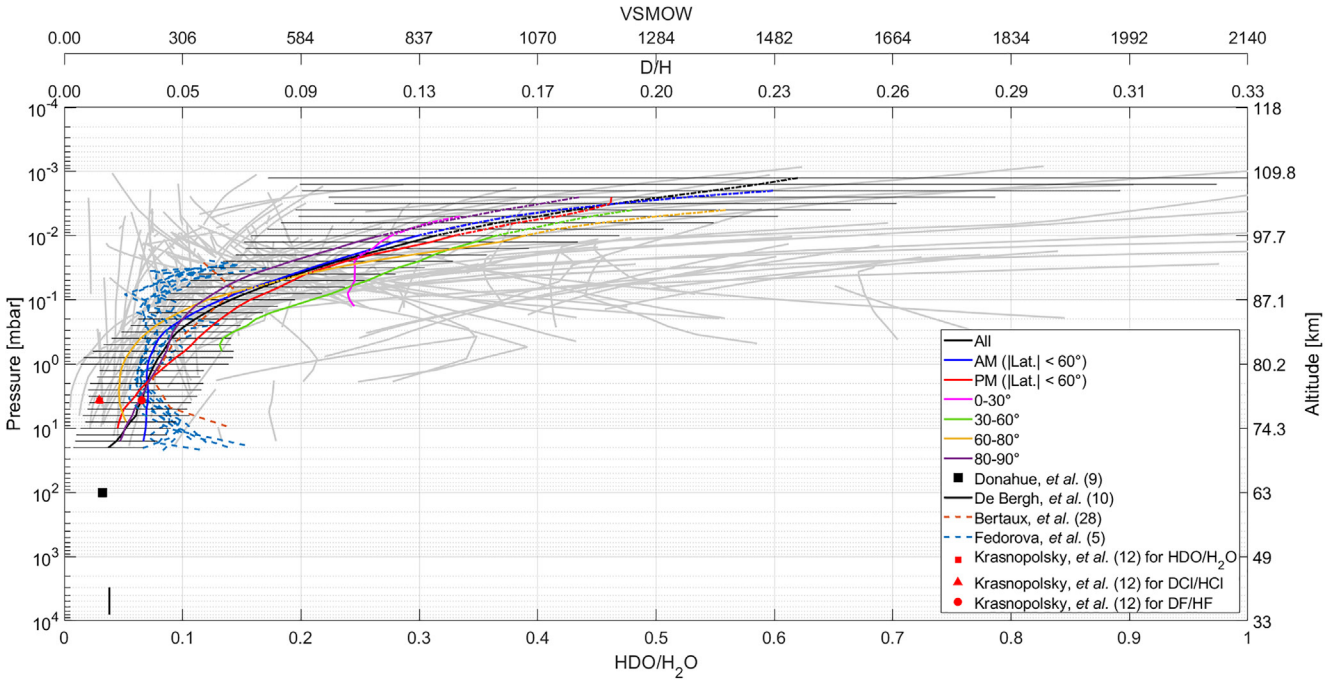

Fig. 2. Individual (gray profiles) and mean (colored profiles, see legend) HDO/H_2O ratio (bottom x-scale), D/H ratio, and factor to VSMOW (top x-scales) from this work and the literature. The horizontal lines represent the weighted variability of the mean profile for the whole database (black curve, "All"). The mean HDO/H_2O profiles above 10^{-2} mbar are set as dashed lines to indicate the larger uncertainty due to the sampling bias explained in the text. The values from the literature are also reported (5, 9, 10, 12, 28).

differences with refs. 5 and 28. The more significant changes are the following:

(i) A reliable order-dependent AOTF transfer function which was not available at the time (34);
(ii) Corrections for the computation of the measured transmittance spectra and noise levels (35);
(iii) A new inversion scheme for the number density retrieval; see section 1.1 (30);
(iv) Considering the calculated temperature profile during the retrieval (30).

Discussion

For the discussion, we consider the SOIR mean temperature profile from Fig. 1*B*, which is reproduced in Fig. 3*A*. This profile is limited to the 75 to 110 km altitude range since the mean polar and lower-latitude temperature profiles show different average values at altitudes below 75 km, and the HDO and H_2O mean profiles were not measured at higher altitudes. We note that the warm layer observed in the 95 to 110 km region, also observed on the Venus night side in the same altitude range (36), remains unexplained by Global Circulation Models (37). The mean SOIR temperature profile is very different from the profiles used in most of the previous studies (18, 19, 21, 24, 25), which are based on the VIRA model.

The SOIR H_2O and HDO profiles presented in *Results* exhibit two main characteristics. First, contrary to early findings (28), we observe increasing H_2O and HDO VMRs with altitude, suggesting a potential water source above 100 km. Second, there is a substantial increase in the HDO/H_2O ratio between 80 and 110 km. This trend was only modestly suggested by previous works (5, 28) while it is significantly more pronounced in the results presented here.

It has been suggested that the latter might result from differential photodissociation (38). Fig. 3*B* shows that the ratio between the photolysis rates of HDO and H_2O drops with decreasing altitude from 0.6 at 110 km to 0.21 at 75 km (see *SI Appendix*, section D for details on the calculation). Fig. 3*C* displays the loss rates corresponding to the product of the photolysis rates by the mean number densities. The photolysis rate ratio is slightly smaller than the one reported in ref. 38, and the loss rates show that it is always larger for H_2O than for HDO. To verify whether photolysis could explain the observed SOIR mean observations, Fig. 3*F* compares the photochemical timescales ($\tau_{\text{photo}} = 1/J$) with the vertical transport timescale [$\tau_{K_{zz}} = H^2/K_{zz}$, where H is the scale height and K_{zz} the eddy diffusion coefficient (41)]. The vertical transport timescale is always at least one order of magnitude smaller than the water photolysis timescales. Because vertical diffusion dominates photolytic destruction, the significant enhancement in the HDO/H_2O ratio observed in the SOIR profiles cannot be accounted for by fractionation due to preferential photolysis. Moreover, this process cannot explain the observed increase of H_2O and HDO VMRs with altitude. Instead, a source for both H_2O and HDO in the gas phase above 90 km is indicated.

Mesospheric water is also present as dihydrate sulfuric $H_2SO_4{\cdot}2H_2O$ aerosols in the upper-haze layer (18). The concentration of deuterium in these aerosols, whether as $HDSO_4$ or HDO, remains unknown. To investigate the role of these aerosols in the increasing H_2O and HDO VMRs and HDO/H_2O ratio profile, we consider the bimodal mean aerosol profiles computed from measurements obtained by SPICAV-UV on board the VEx spacecraft in solar occultation mode between 80 and 100 km (39); see Fig. 3*D*. For the sake of simplicity, we assume an altitude-constant effective radius of 0.12 μm for aerosol mode 1 and 0.8 μm for mode 2 based on that work. These measurements were taken at the same LST—the terminator region—and during the

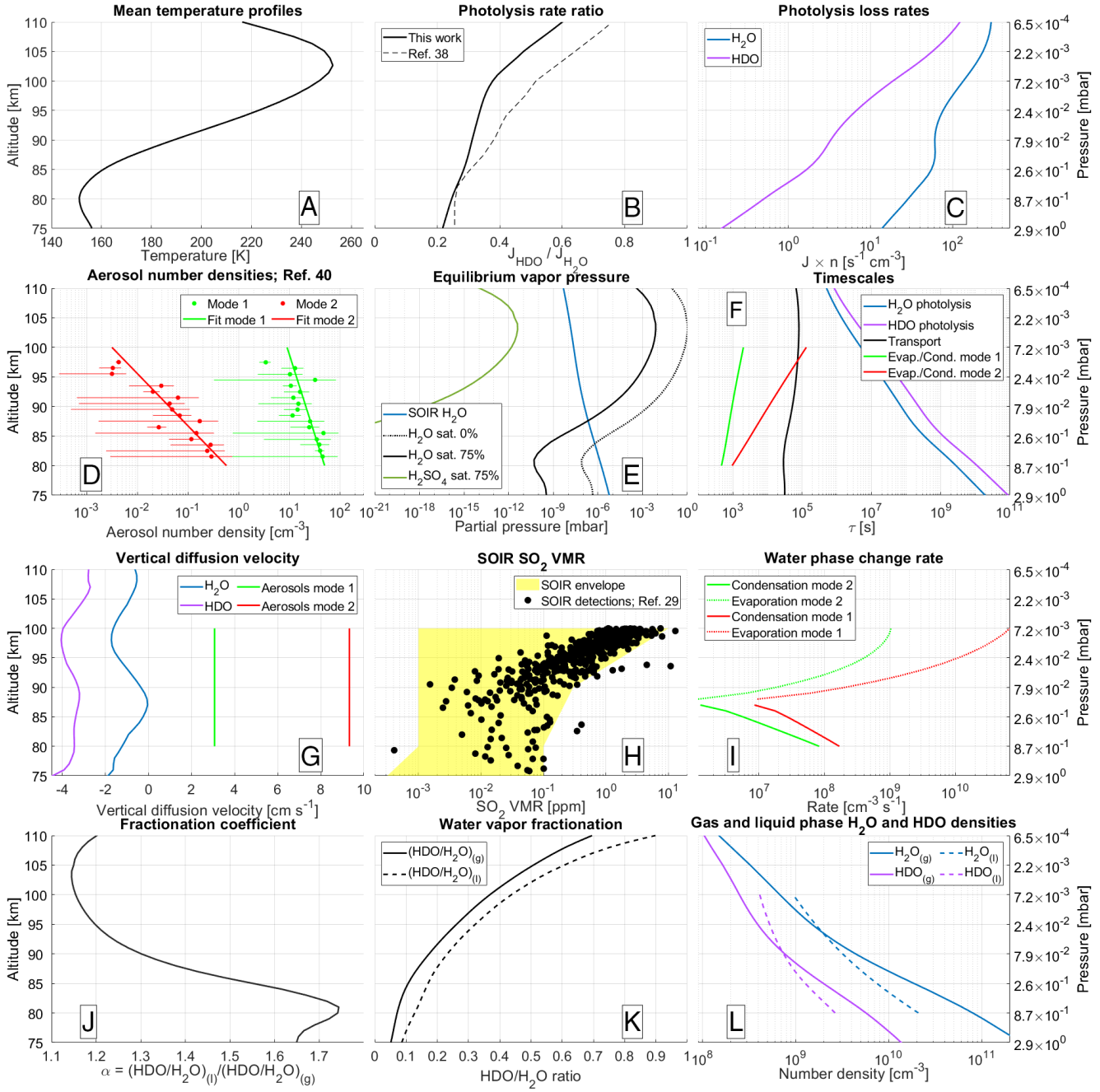

Fig. 3. (Panel *A*) Mean SOIR temperature profile, as in Fig. 1*B*. (Panel *B*) Ratio of the HDO and H_2O photolysis rates considering the UV cross-sections; see *SI Appendix*, section D. The ratio of the photolysis rates from ref. 38 is also reported. (Panel *C*) H_2O and HDO loss rates. (Panel *D*) Modes 1 and 2 aerosol number densities from ref. 39 and exponential fit of the profiles (straight lines). (Panel *E*) Comparison of the SOIR mean H_2O partial pressure profile, the pure H_2O equilibrium vapor pressure profile (H_2O sat 0%), and the H_2O equilibrium vapor pressure profile in 75% H_2SO_4 in mass (H_2O sat. 75%) computed from ref. 40 considering the SOIR mean temperature profile from Panel *A*, and the H_2SO_4 equilibrium vapor pressure profile in 75% H_2SO_4 in mass (H_2SO_4 75%). (Panel *F*) Transport, H_2O and HDO photochemical, and aerosol phase change timescales τ computed from the eddy diffusion coefficient, the photolysis rates, and the aerosols number densities and effective radii from ref. 39 displayed in Panel *D*. The eddy diffusion coefficient K_{zz} is taken from ref. 41, while the photolysis rates are the ones of Panel *B*. The computation of the phase change rates is given in *SI Appendix*, section E. (Panel *G*) Vertical velocity of H_2O, HDO, and the aerosols (39) computed from the vertical fluxes. (Panel *H*) SOIR SO_2 detections from ref. 29 and envelope of those detections. (Panel *I*) Rate of water vapor phase change computed for both modes of aerosols. (Panel *J*) Fractionation due to condensation of H_2O and HDO (42). (Panel *K*) HDO/H_2O ratio for pure water vapor in gas and liquid phases (42). (Panel *L*) Mean H_2O and HDO vertical number density profiles from SOIR and pure H_2O and HDO in equilibrium liquid phase considering the fractionation coefficient from Panels *J* and *K* (42). The corresponding pressure scale is given on the right-hand side of Panels *C*, *F*, *I*, and *L*.

same time period as the SOIR observations. Also, we assume an altitude-constant concentration of 75% H_2SO_4 and 25% H_2O by mass in the aerosol particles, corresponding to mole fractions of 35.5% for H_2SO_4 and 64.5% for H_2O. This approximation is based on the findings of ref. 43, who reported minor variations with altitude of the mass fraction of H_2SO_4 (~75%). We note that a portion of the aerosols could also contain polysulfur S_x (19). However, this study shows that even though a fraction of the aerosols may consist of polysulfur, a more significant fraction is likely composed of sulfuric acid above 80 km.

Measurements of gas-phase H_2SO_4 from the Venus Radio Occultation experiment on board VEx were obtained between 38 and 55 km (44). This altitude range is lower than the region addressed in this work. Indeed, photochemical models suggest

that the H_2SO_4 VMR is expected to be low and thus undetectable above 55 km, even considering H_2SO_4 supersaturation (18, 24). Additionally, no measurements or modeling of $HDSO_4$ have been reported in the literature.

Fig. 3*E* compares the SOIR mean H_2O partial pressure with both the equilibrium vapor pressure of pure H_2O and that of H_2O in a mixture containing 75% H_2SO_4 and 25% H_2O by mass (ref. 40 and references therein). The equilibrium vapor pressure of H_2SO_4 in the same mixture is also reported. We observe that the equilibrium vapor pressure of H_2O in this mixture is reduced by more than two orders of magnitude compared to that of pure liquid water. H_2O condensation occurs below 87 km, while evaporation occurs at higher altitudes, leading to an increase in the H_2O VMR in that region. The evaporation rate is function of the difference between the water vapor partial pressure and the equilibrium vapor pressure (*SI Appendix*, Eq. **S4**) and is displayed in Fig. 3*I*, which increases with altitude between 87 km and 103 km and supports the increase in water vapor partial pressure with altitude. Based on the straightforward approach presented in this work, water vapor supersaturation could be expected below 87 km, similar to the possible H_2SO_4 supersaturation already identified in several modeling studies (18, 19, 25).

We compute the timescale of the aerosol phase changes (see Fig. 3*F* and *SI Appendix*, section E for details on the computation). We find that they increase with altitude by a factor of four for mode 1 and by two orders of magnitude for mode 2. Under steady-state conditions, the phase change for mode 1 is always faster than transport by one to two orders of magnitude, while the phase change for mode 2 is faster than transport below 98 km by up to approx. one order of magnitude and becomes slower above that altitude. For both modes, condensation occurring below 87 km is always faster than transport. These aspects justify the increase of the water vapor VMR with altitude at steady-state conditions.

We calculate the vertical diffusion velocities of H_2O and HDO considering the SOIR mean number density and temperature profiles, using the vertical fluxes computed from the minor species approximation (*SI Appendix*, section F and Fig. 3*G*). As expected, our results reveal downward diffusion for both H_2O and HDO resulting from their VMR vertical gradients. Specifically, the H_2O diffusion velocity varies between ~0 and −1.9 cm/s, while it ranges from −2.8 and −4.4 cm/s for HDO. Notably, the latest is at least twice as fast as that of H_2O. We also compute the aerosol vertical diffusion velocity and find upward diffusion speeds of 3 cm/s for mode 1 and 9.3 cm/s for mode 2 (see *SI Appendix*, section F for details on the computation). We note that our computations for the aerosols are based solely on the minor species diffusion equation, considering the mean aerosol profiles (39), and do not incorporate parameterizations for factors such as sedimentation, viscous drag, etc.

Combining the rationales on the timescales and the diffusion velocities at steady state, mode 1 aerosols quickly form at altitudes above the cloud deck, and as they diffusively reach altitudes higher than 87 km, they start to evaporate. This evaporation occurs on a timescale shorter than transport, though increasing with altitude. For mode 2, the timescale increases faster with altitude than for mode 1 and remains faster than transport up to 98 km. This fact is reflected in the slope of the mean aerosol profiles of Fig. 3*D*, where we see that mode 2 aerosols have a smaller slope than mode 1.

Through the qualitative reasoning presented earlier and by integrating the discussion on H_2O vertical velocities with the processes involving phase changes of H_2O, we propose a water cycle in the Venusian mesosphere (Fig. 4). This cycle not only aligns with the SOIR observations of H_2O and HDO but also supports the observations of SO_2 in the upper mesosphere (22, 23, 29) (Fig. 3*H*). Notably, these observations reveal an inversion layer above 75 km, where the maximum SO_2 VMR increases by nearly a factor of 10. Many authors have already examined this characteristic from a modeling perspective (19, 45). A key aspect of this cycle is the role of H_2SO_4 photodissociation, which predominantly occurs at these altitudes and leads to the production of sulfur oxides.

We note that the relative water concentration in aerosols adjusts to thermal equilibrium, which is governed by the surrounding atmospheric temperature, leading to altitude-dependent minor variations. For simplicity, these variations are not included in the present work. At ~80 km, where temperatures are lowest, model studies estimated the water concentration in aerosols to be about 20% by mass (43), corresponding to a mole fraction of ~0.58. This indicates that water dominates the aerosol composition. Above ~80 km, as temperatures increase, the water concentration in aerosols is expected to decrease due to changes in thermal equilibrium. Consequently, aerosols originating from below ~80 km are likely to release water during their vertical transport, as shown by recent microphysical modeling using the SOIR temperature profile (26). This water evaporation occurs just above 87 km and increases as the aerosols diffusively ascend to higher altitudes (Fig. 3 *E* and *I*).

To fully test our hypothesis that the increase in H_2O and D/H in the Venusian mesosphere is a result of aerosol transport requires an aerosol microphysical model that incorporates the complex condensation/evaporation processes as well as vertical transport due to winds. Though these models have yet to be developed we note that vigorous convection has been suggested to explain the increase in SO_2 in the Venusian mesosphere. In ref. 21, the possibility of transient vertical wind gusts from the clouds region to an altitude of 70 km is considered in their modeling effort to reproduce the observed SO_2 upper-mesosphere increase (22, 23, 29). These hypothetical winds peak at 70 km with a vertical velocity of ~100 cm/s and lift up aerosols from the cloud region to the mesosphere. This increases the aerosol density at 75 km by nearly two orders of magnitude compared to the nominal aerosol particle number density profile. Ref. 21 also show that in the relaxed situation following the wind gusts, the upper-mesosphere aerosol concentration increases by a factor of 4. These winds would likely extend to higher altitudes as well and may play a role in the transport of aerosols considered here. Because our analysis concentrates on the mean conditions that we assume are in steady state, the strong updrafts (and corresponding downdrafts) should be viewed as contributors to eddy transport. This may help explain the large values of the eddy diffusion coefficient K_{zz} in the upper mesosphere found in ref. 41.

If mesospheric water vapor originates from aerosol evaporation between ~87 and ~115 km, these aerosols should be enriched in deuterium. Deuterated species are known to condense more readily than their hydrogenated counterparts (42), resulting in an isotopic fractionation with a higher deuterium concentration in the condensed phase. Fractionation coefficients for pure water are available in the literature (42), but these have not been found for an $H_2SO_4{\cdot}2H_2O$ mixture. Previous studies demonstrated that acids and salts in aqueous solutions increase deuterium fractionation (46). Therefore, we consider the temperature-dependent expression of pure water fractionation as an upper bound for the fractionation of water in an $H_2SO_4{\cdot}2H_2O$ mixture. The fractionation coefficient is defined as

$$\alpha = \left(\frac{\mathrm{HDO}}{\mathrm{H_2O}}\right)_l \Big/ \left(\frac{\mathrm{HDO}}{\mathrm{H_2O}}\right)_g, \qquad [2]$$

where the subscript *l* refers to the liquid phase and the *g* refers to the gas phase (Fig. 3*J*). We compute the fractionation profiles in the liquid phase of water based on the mean HDO/H_2O ratio in the gas phase shown in Fig. 2; see Fig. 3*K*. The resulting number density profiles of H_2O and HDO in the liquid phase are reported in Fig. 3*L*, together with their equivalent in the gas phase. We

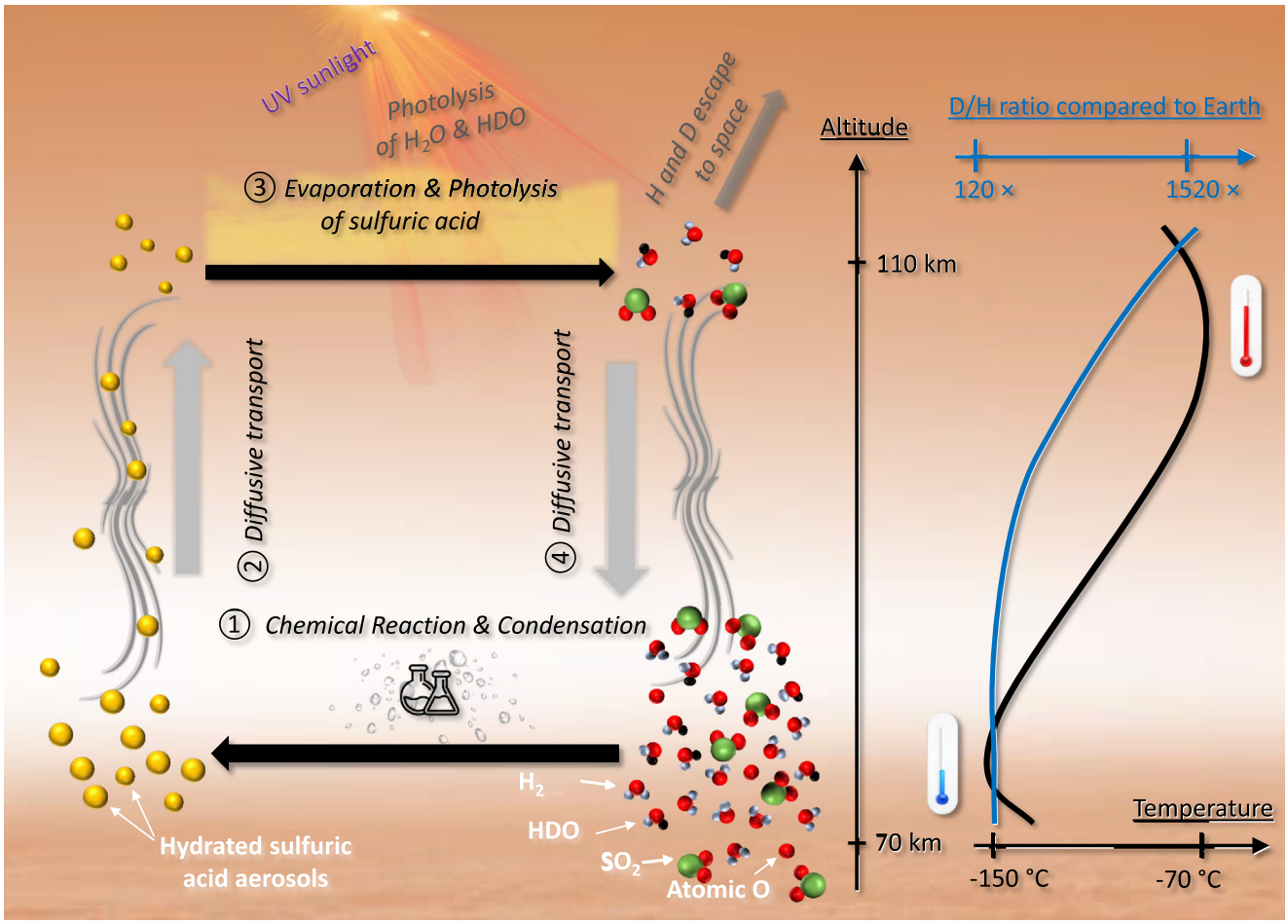

Fig. 4. Cartoon of the proposed Venus mesospheric water cycle mechanism to sustain the observed increase in HDO and H_2O VMR and HDO/H_2O ratio with altitude: fractionation during H_2O and HDO condensation process above the cloud top, upwelling of the aerosols, evaporation above ~85 km and increase of the H_2O, HDO, and SO_2 VMRs and the HDO/H_2O ratio, and downwelling of H_2O and HDO.

note that, under the assumptions described above, they are of the same order of magnitude. The fractionation coefficient varies between ~1.7 at 75 km to ~1.15 at 110 km. This variation indicates that the HDO/H_2O ratio in the liquid phase decreases with altitude compared to the gas phase, a trend also observed in the liquid phase HDO and H_2O profiles in Fig. 3*L*.

In summary, it appears that the condensation-induced deuterium enrichment of aerosols formed above the clouds and transported to higher altitudes where they evaporate could be a key mechanism driving both the observed increase of the H_2O and HDO VMR with altitude as well as the concurrent rise in deuterated water. All processes controlling the proposed mechanism are summarized in Fig. 4, namely

(i) condensation-induced isotopic fractionation leading to a deuterium enrichment in $H_2SO_4 \cdot 2H_2O$ aerosols above the cloud top where the temperature is lower than the dew point;
(ii) upward diffusion of these droplets to altitudes higher than 100 km;
(iii) evaporation of the deuterium-enriched aerosols due to the higher temperatures, inducing an increase of the H_2O and HDO VMR and the HDO/H_2O ratio;
(iv) downward diffusion of H_2O and HDO;
(v) as proposed previously (19, 21), this cycle should also lead to an enhancement in SO_2 above ~85 km, which is observed by SOIR (22, 23, 29) and SPICAV (47).

Accurately modeling the aerosol condensation and evaporation and its influence on D/H fractionation goes beyond the scope of this work. It will be addressed in future work, as it requires the use of microphysical aerosol models. Also, isotopic fractionation may occur during chemical reactions producing H_2SO_4 and $HDSO_4$, as well as during their condensation together with H_2O and HDO to form the aerosol particles. Future experimental studies should thus be conducted to determine the rates of these processes.

The large vertical variation in the D/H ratio found in this study has not been previously considered in investigations of atmospheric evolution on Venus (9). Our results have two major implications for evolutionary studies. First, the altitude variation of D/H must be taken into account when computing the net reservoirs of D and H residing in the atmosphere (48) and relating that to the initial reservoir. Second, and perhaps of more interest, the processes responsible for the altitude variation in D/H likely alter the relative escape rates of H and D. For example, in the present-day atmosphere, photolysis of H_2O and HDO occurs mainly at altitudes above ~100 km, where the D/H ratio is nearly 1,000 VSMOW. Thus, far more D is liberated by photolysis than would be expected based on the VMR in the deep atmosphere. If any fraction of this liberated D escapes, it could significantly alter the evolution of the D/H ratio. It follows that evolutionary models must include the physical processes responsible for the altitude variation to calculate the D/H fractionation accurately.

Estimating water loss from the Venusian atmosphere cannot be straightforwardly deduced from the current atmospheric D/H ratio

profile (49), as it requires complex modeling. This work opens the door for future work that could significantly advance our understanding of the intricate processes governing Venus's atmospheric chemistry and the water cycle in the Venus mesosphere. It also aims to provide constraints on the hydrogen and deuterium escape processes and shed light on the amount of water Venus has had in the past.

Materials and Methods

The SOIR spectrometer characteristics, the spectroscopy, and an example of retrieval are provided in *SI Appendix*. To discuss the SOIR results presented in this work, we consider well-established equations and physical laws. The photolysis rates are computed by spectrally integrating the product of the absorption cross sections, the quantum yields, the transmittance, and the solar flux scaled for Venus. The evaporation and condensation partial pressures and rates are computed considering the difference between the measured mean water vapor abundances and the saturation pressures for a $H_2O{\cdot}2H_2SO_4$ mixture at the local temperature, the diffusion coefficient of water in a CO_2 background, and the correction factor function of the Knudsen number (50). Finally, we use the minor species approximation to compute the water and aerosol vertical fluxes.

Data, Materials, and Software Availability. Number density and temperature vertical profiles data have been deposited in VESPA (https://doi.org/10.18758/71021090) (51).

ACKNOWLEDGMENTS. Venus Express is a planetary mission from the ESA. We wish to thank all ESA members who participated in the mission. The research program was supported by the Belgian Federal Science Policy Office and the ESA (PRODEX program, contracts C 90268, 90113, and 17645). The research leading to these results has received funding from the European Union Seventh Framework Program (FP7/2007-2013) under grant agreement no. 606798. A.M. was supported by the Marie Skłodowska-Curie Action from the European Commission under grant number 838587. A.P., S.R., J.T.E., and S.V. thank Belspo for the Brain, FED-tWIN, and PRODEX fundings (B2/233/P2/VAMOS, B2/191/P1/MICROBE, Prf-2019-077–RT-MOLEXO, and PRODEX contracts no. 4000137943 and 4000144206). H.N. was supported by the Japan Society for the Promotion of Science (JSPS) KAKENHI Grant Number JP22KK0044. H.K. was supported by the JSPS KAKENHI Grant Numbers JP23KJ0201 and the International Joint Graduate Program in Earth and Environmental Sciences of Tohoku University. The Europlanet-2024 Research Infrastructure project has received funding from the European Union's Horizon 2020 research and innovation program under grant agreement no. 871149.

Author affiliations: [a]Division of Planetary Atmosphere, Royal Belgian Institute for Space Aeronomy, Brussels 1180, Belgium; [b]Computational Flow Physics Laboratory, Department of Aerospace Engineering and Engineering Mechanics, The University of Texas at Austin, Austin, TX 78712; [c]Lunar and Planetary Laboratory, University of Arizona, Tucson, AZ 85721; and [d]Graduate School of Science, Department of Geophysics, Tohoku University, Sendai 980-8576, Japan

1. B. Bézard, A. Fedorova, J. L. Bertaux, A. Rodin, O. Korablev, The 1.10- and 1.18-μm nightside windows of Venus observed by SPICAV-IR aboard Venus Express. *Icarus* **216**, 173–183 (2011).
2. D. C. Catling, J. F. Kasting, *Atmospheric Evolution on Inhabited and Lifeless Worlds* (Cambridge University Press, Cambridge, 2017).
3. T. Encrenaz, R. Moreno, A. Moullet, E. Lellouch, T. Fouchet, Submillimeter mapping of mesospheric minor species on Venus with ALMA. *Planet. Space Sci.* **113–114**, 275–291 (2015).
4. C. Tsang, T. Encrenaz, C. N. DeWitt, M. Richter, P. Irwin, Airborne measurements of Venus cloud-top H_2O and HDO from NASA's SOFIA in the mid-infrared (meeting #49, id.502.04, Division for Planetary Science (DPS), American Astronomical Society, Provo, UT, 2017), p. 502.504.
5. A. Fedorova *et al.*, HDO and H_2O vertical distributions and isotopic ratio in the Venus mesosphere by solar occultation at infrared spectrometer onboard Venus Express. *J. Geophys. Res.* **113**, E00B22 (2008).
6. S. Chamberlain *et al.*, SOIR/VEx observations of water vapor at the terminator in the Venus mesosphere. *Icarus* **346**, 113819 (2020).
7. V. Cottini, N. I. Ignatiev, G. Piccioni, P. Drossart, Water vapor near Venus cloud tops from VIRTIS-H/Venus Express observations 2006–2011. *Planet. Space Sci.* **113–114**, 219–225 (2015).
8. V. Krasnopolsky, J. B. Pollack, H_2O–H_2SO_4 system in Venus' clouds and OCS, CO and H_2SO_4 profiles in Venus troposphere. *Icarus* **109**, 58–78 (1994).
9. T. M. Donahue, J. H. Hoffman, R. R. Hodges, A. J. Watson, Venus was wet–A measurement of the ratio of deuterium to hydrogen. *Science* **216**, 630–633 (1982).
10. C. de Bergh, Deuterium on Venus–Observations from Earth. *Science* **251**, 547–549 (1991).
11. M. A. Gurwell, G. J. Melnick, V. Tolls, E. A. Bergin, B. M. Patten, SWAS observations of water vapor in the Venus mesosphere. *Icarus* **188**, 288–304 (2007).
12. V. A. Krasnopolsky, D. A. Belyaev, I. E. Gordon, G. Li, L. S. Rothman, Observations of D/H ratios in H_2O, HCl, and HF on Venus and new DCl and DF line strengths. *Icarus* **224**, 57–69 (2013).
13. L. J. Hallis, D/H ratios of the inner solar system. *Phil. Trans. R. Soc. A* **375**, 20150390 (2017).
14. L. Yang, F. J. Ciesla, C. M. O. D. Alexander, The D/H ratio of water in the solar nebula during its formation and evolution. *Icarus* **226**, 256–267 (2013).
15. H. Nomura *et al.*, "The isotopic links from planet forming regions to the solar system" in *Protostars and Planets VII* (ASP Conference Series, University of Arizona Press, 2023), pp. 1075–1099.
16. M. S. Chaffin *et al.*, Venus water loss is dominated by HCO^+ dissociative recombination. *Nature* **629**, 307–310 (2024).
17. M. Turbet *et al.*, Day–night cloud asymmetry prevents early oceans on Venus but not on Earth. *Nature* **598**, 276–280 (2021).
18. X. Zhang, M. Liang, F. Mills, D. Belyaev, Y. Yung, Photolysis of sulphuric acid as the source of sulphur oxides in the mesosphere of Venus. *Nat. Geosci.* **3**, 834–837 (2010).
19. X. Zhang, M. Liang, F. Mills, D. Belyaev, Y. Yung, Sulfur chemistry in the middle atmosphere of Venus. *Icarus* **217**, 714–739 (2012).
20. R. G. Knollenberg, D. M. Hunten, The microphysics of the clouds of Venus: Results of the Pioneer Venus particles and size spectrometer experiment. *J. Geophys. Res.* **85**, 8039–8058 (1980).
21. P. Gao, X. Zhang, D. Crisp, C. G. Bardeen, Y. L. Yung, Bimodal distribution of sulfuric acid aerosols in the upper haze of Venus. *Icarus* **231**, 83–99 (2014).
22. D. Belyaev *et al.*, Vertical profiling of SO_2 and SO above Venus' clouds by SPICAV/SOIR solar occultations. *Icarus* **217**, 740–751 (2012).
23. A. Mahieux *et al.*, Venus mesospheric sulfur dioxide measurement retrieved from SOIR on board Venus Express. *Planet. Space Sci.* **113–114**, 193–204 (2015).
24. V. Krasnopolsky, Vertical profiles of H_2O, H_2SO_4, and sulfuric acid concentration at 45–75 km on Venus. *Icarus* **252**, 327–333 (2015).
25. K. McGouldrick, O. B. Toon, An investigation of possible causes of the holes in the condensational Venus cloud using a microphysical cloud model with a radiative-dynamical feedback. *Icarus* **191**, 1–24 (2007).
26. H. Karyu, One-dimensional microphysics model of Venusian clouds from 40 to 100 km: Impact of the middle-atmosphere eddy transport and SOIR temperature profile on the cloud structure. *Planet. Sci. J.* **5**, 57 (2024).
27. A. Mahieux, S. Robert, A. Piccialli, L. Trompet, A. C. Vandaele, The SOIR/Venus Express species concentration and temperature database: CO_2, CO, H_2O, HDO, $H^{35}Cl$, $H^{37}Cl$, HF individual and mean profiles. *Icarus* **405**, 115713 (2023).
28. J. L. Bertaux, A warm layer in Venus' cryosphere and high altitude measurements of HF, HCl, H_2O and HDO. *Nature* **450**, 646–649 (2007).
29. A. Mahieux *et al.*, Update on SO_2, detection of OCS, CS, CS_2, and SO_3, and upper limits of H_2S and HOCl in the Venus mesosphere using SOIR on board Venus Express. *Icarus* **399**, 115556 (2023).
30. A. Mahieux *et al.*, Densities and temperatures in the Venus mesosphere and lower thermosphere retrieved from SOIR onboard Venus Express: Retrieval technique. *J. Geophys. Res.* **115**, 1–15 (2010).
31. L. V. Zasova, N. I. Ignatiev, I. Khatuntsev, V. Linkin, Structure of the Venus atmosphere. *Planet. Space Sci.* **55**, 1712–1728 (2007).
32. J. B. Pollack, Near-infrared light from Venus' nightside: A spectroscopic analysis. *Icarus* **103**, 1–42 (1993).
33. S. Limaye, The thermal structure of the Venus atmosphere: Intercomparison of Venus Express and ground based observations of vertical temperature and density profiles. *Icarus* **294**, 124–155 (2017).
34. A. Mahieux, A new method for determining the transfer function of an Acousto optical tunable filter. *Opt. Express* **17**, 2005–2014 (2009).
35. L. Trompet, Improved algorithm for the transmittance estimation of spectra obtained with SOIR/Venus Express. *Appl. Opt.* **55**, 9275–9281 (2016).
36. A. Piccialli, Thermal structure of Venus upper atmosphere measured by stellar occultations with SPICAV/Venus Express. *Planet. Space Sci.* **113–114**, 321–335 (2015).
37. S. W. Bougher, Upper atmosphere temperature structure at the Venusian Terminators: A comparison of SOIR and VTGCM results. *Planet. Space Sci.* **113–114**, 336–346 (2015).
38. M. C. Liang, Y. L. Yung, Modeling the distribution of H_2O and HDO in the upper atmosphere of Venus. *J. Geophys. Res.* **114**, 1–9 (2009).
39. M. Luginin, Bimodal aerosol distribution in Venus' upper haze from joint SPICAV-UV and -IR observations on Venus Express. *Icarus* **409**, 115866 (2024).
40. T. Imamura, G. L. Hashimoto, Venus cloud formation in the meridional circulation. *J. Geophys. Res.* **103**, 31349–31366 (1998).
41. A. Mahieux, Determination of the Venus eddy diffusion profile from CO and CO_2 profiles using SOIR/Venus Express observations. *Icarus* **361**, 114388 (2021).
42. L. Merlivat, G. Nief, Fractionnement isotopique lors des changements d'état solide-vapeur et liquide-vapeur de l'eau à des températures inférieures à 0°C. *Tellus A* **19**, 122–127 (1967).
43. A. Stolzenbach, Three-dimensional modeling of Venus photochemistry and clouds. *Icarus* **395**, 115447 (2023).
44. J. Oschlisniok, Sulfuric acid vapor and sulfur dioxide in the atmosphere of Venus as observed by the Venus Express radio science experiment VeRa. *Icarus* **362**, 114405 (2021).
45. C. Parkinson, Distribution of sulphuric acid aerosols in the clouds and upper haze of Venus using Venus Express VAST and VeRa temperature profiles. *Planet. Space Sci.* **113–114**, 205–218 (2015).
46. M. K. Stewart, I. Friedman, Deuterium fractionation between aqueous salt solutions and water vapor. *J. Geophys. Res.* **80**, 3812–3818 (1975).
47. D. Evdokimova, The spatial and temporal distribution of nighttime ozone and sulfur dioxide in the Venus mesosphere as deduced from SPICAV UV stellar occultations. *J. Geophys. Res.* **126**, e2020JE006625 (2021).
48. D. H. Grinspoon, Implications of the high D/H ratio for the sources of water in Venus' atmosphere. *Nature* **363**, 428–431 (1993).
49. C. Gillmann, The long-term evolution of the atmosphere of Venus: Processes and feedback mechanisms. *Space Sci. Rev.* **218**, 56 (2022).
50. N. A. Fuchs, A. G. Sutugin, "High-dispersed aerosols" in *Topics in Current Aerosol Research*, G. M. Hidy, J. R. Brock, Eds. (Pergamon, 1971), p. 1, 10.1016/B978-0-08-016674-2.50006-6.
51. L. Trompet, A. Mahieux, A. C. Vandaele, Virtual European Solar and Planetary Access. Venus atmospheric profiles - From SPICAV-SOIR/Vex. https://vespa.obspm.fr/planetary/data/display/?&service_id=ivo://bira-iasb/soir/soir_q/epn_core&service_type=epn. Deposited 17 January 2024.